Available online at www.sciencedirect.com
ScienceDirect
Journal of the European Ceramic Society 30 (2010) 2375–2386
www.elsevier.com/locate/jeurceramsoc

In situ studies of oxidation of ZrB_2 and ZrB_2–SiC composites at high temperatures

P. Sarin, P.E. Driemeyer, R.P. Haggerty, D.-K. Kim, J.L. Bell, Z.D. Apostolov, W.M. Kriven *

Department of Materials Science and Engineering, University of Illinois at Urbana-Champaign, 1304 West Green Street, Urbana, IL 61801, USA

Available online 15 April 2010

Abstract

High temperature oxidation of ZrB_2 and the effect of SiC on controlling the oxidation of ZrB_2 in ZrB_2–SiC composites were studied in situ, in air, using X-ray diffraction. Oxidation was studied by quantitatively analyzing the crystalline phase changes in the samples, both non-isothermally, as a function of temperature, up to ~1650 °C, as well as isothermally, as a function of time, at ~1300 °C. During the non-isothermal studies, the formation and transformation of intermediate crystalline phases of ZrO_2 were also observed. The change in SiC content, during isothermal oxidation studies of ZrB_2–SiC composites, was similar in the examined temperature range, regardless of sample microstructure and composition. Higher SiC content, however, markedly retarded the oxidation rate of the ZrB_2 phase in the composites. A novel approach to quantify the extent of oxidation by estimating the thickness of the oxidation layer formed during oxidation of ZrB_2 and ZrB_2–SiC composites, based on fractional conversion of ZrB_2 to ZrO_2 in situ, is presented.

Keywords: Ultra-high temperature ceramics; X-ray methods; Borides; ZrB_2; SiC; Oxidation

1. Introduction

Transition metal diborides have been subjects of extensive research in the last decade as ultra-high temperature ceramics (UHTC's) for applications such as thermal protection systems on re-usable atmospheric re-entry vehicles and on scramjet engine components for hypersonic aerospace vehicles.[1–6] These materials exhibit a unique combination of thermo-mechanical properties which make them attractive candidates for aerospace applications under extreme environments. Zirconium diboride (ZrB_2) is one such UHTC which has been studied because of its extremely high melting temperature ($T_{melt} > 3040$ °C), high elastic modulus, high electrical and thermal conductivity, good thermal shock and wear resistance, and chemical inertness.[7–11] The superior high temperature properties are primarily due to strong covalent bonding in the ZrB_2 structure.[11] Extremely low self-diffusion coefficients, on the other hand, make processing of dense ZrB_2 ceramics a challenge. Pure ZrB_2 is typically sintered around 2000 °C under an applied load in a controlled atmosphere furnace.[12] Numerous studies have focused on the use of alternate sintering methods to achieve dense ZrB_2 ceramics, such as by using sintering aids, by reactive routes or by spark plasma sintering.[11] Another major challenge in the development of ZrB_2 UHTCs lies in their poor resistance to oxidation which severely undermines their ability to survive oxidizing conditions at high temperatures.

When exposed to air, crystalline ZrB_2 oxidizes to ZrO_2 and B_2O_3 according to reaction (1).[13] At temperatures less than 1100 °C, the B_2O_3 forms a continuous liquid layer which limits the transport of oxygen to the ZrB_2 surface, and as a consequence diffusion controlled, parabolic, oxidation kinetics are observed.[14–19] The ZrO_2 formed on oxidation of ZrB_2 is porous and therefore non-protective towards further oxidation:

$$ZrB_2 + \tfrac{5}{2}O_2(g) \rightarrow ZrO_2 + B_2O_3(l) \quad (1)$$

Based on thermo-gravimetric analysis (TGA), at temperatures above 1100 °C, the oxidation rate increases and exhibits para-linear kinetics between 1100 and 1400 °C. In this temperature range, the mass change is determined by (a) weight gain due to the formation of B_2O_3 and ZrO_2 and (b) weight loss due to vaporization of B_2O_3 (l).[17,18] At temperatures higher than 1400 °C, linear oxidation kinetics ensue due to rapid evaporation of B_2O_3, and a non-protective porous ZrO_2 scale is formed.[20,21] Overall, a net gain in mass is observed.

* Corresponding author. Tel.: +1 217 333 5258; fax: +1 217 333 2736.
E-mail address: kriven@illinois.edu (W.M. Kriven).

0955-2219/$ – see front matter © 2010 Elsevier Ltd. All rights reserved.
doi:10.1016/j.jeurceramsoc.2010.03.009

The addition of silica scale formers, such as SiC or $MoSi_2$, has been shown to improve oxidation resistance above 1100 °C.[19,22–27] The inclusion of SiC results in the formation of a silica (SiO_2) based glassy layer on the ZrB_2–SiC composite surfaces. The SiO_2 layer is less volatile than B_2O_3 above 1100 °C, resulting in slow, diffusion-controlled oxidation kinetics in ZrB_2–SiC composites over a much greater temperature range.[23] Moreover, SiC acts as a grain growth inhibitor, increasing sinterability, and thus improving strength, toughness, and oxidation resistance of the composite.[6,8,17,22,23,28,29]

Oxidation of ZrB_2–SiC at 1500 °C produces a multilayered microstructure consisting of a surface scale that is SiO_2 rich, followed by a layer of non-oxidized ZrB_2 over the underlying ZrB_2–SiC composite. In addition, a layer composed of crystalline ZrO_2 has also been reported between the silica-rich surface layer and the non-oxidized ZrB_2 layer.[6,30,31] The formation of such a layered structure exhibiting a "SiC-depleted" region above the ZrB_2–SiC bulk composite during oxidation has been noted by several authors.[19,20,23,24,30] The absence of SiO_2 or other condensed phases in the SiC-depleted zone has been explained by its removal as gaseous phases such as SiO.[30]

Most of the current understanding on the oxidation of ZrB_2 and ZrB_2–SiC composites is based on thermo-gravimetric studies, oxygen consumption studies and on ex situ evaluation of microstructural changes. While thermo-gravimetric methods provide useful information based on weight changes during oxidation, they record the simultaneous occurrence of multiple events including weight gain due to formation of oxide phases, such as ZrO_2, B_2O_3 and SiO_2, and weight loss due to vaporization of B_2O_3 and perhaps SiO. As a result, the TGA data needs to be deconvoluted and requires careful interpretation. The post-oxidation, ex situ analysis of microstructure, on the other hand, is largely qualitative and limited in knowledge of the oxidation phenomena and reactions, as they occur. The oxidation and the scale formation in the UHTC diborides involve the complex interaction of a number of factors. The resulting multiphase, multilayered scale microstructure makes it even more difficult to determine the factors that control oxygen transport during the oxidation of the composites. In order to realize the full potential of UHTC diborides for advanced hypersonic and propulsion applications, and to improve their oxidation resistance, a more comprehensive understanding of the oxidation process is desired.

In situ high temperature investigation of the oxidation of UHTC diborides using X-ray diffraction can provide a clearer insight into the oxidation kinetics and structure-property relationships. Although such studies are extremely challenging due to instrumental limitations, they can lead to improved life prediction of UHTC components and perhaps indicate an optimal composite through tailoring of composition and microstructure. This study was aimed at evaluating the use of high temperature X-ray diffraction (HTXRD) to examine the oxidation of ZrB_2 up to ~1650 °C in air. The effect of SiC on the oxidation of ZrB_2 in ZrB_2–SiC composites was also evaluated. A specially designed quadrupole lamp furnace (QLF), which allows heating of samples up to 2000 °C in air,[32–35] was used in conjunction with a high resolution curved image plate (CIP) detector for these studies.[36,37] Using this method, the oxidation of ZrB_2 to ZrO_2 was monitored in real time, independent of other accompanying processes.

2. Experimental procedure

2.1. Sample processing

Commercially available ZrB_2 (Aldrich Chemical Company, Milwaukee, WI, USA) with a reported purity of 95% (purity excludes 1–2% Hf), density of 6.08 g/cm^3, and an averaged particle size of 5 μm was used. The SiC powder (Aldrich Chemical Company, Milwaukee, WI, USA) used in this study was predominantly β-SiC (3–15% amorphous), had a density of 3.22 g/cm^3, an average particle size <0.1 μm and specific surface area of 70–90 m^2/g. While the pure ZrB_2 sample was made using the commercially available powder, two ZrB_2–SiC composites were prepared by mixing batches of commercial powders of ZrB_2 and SiC in proportion such that the final samples had ZrB_2 and SiC in the ratios 70:30 and 50:50 by volume, respectively. The powder batches for the composite samples were ball milled for 24 h, using 3Y-TZP (3 mol% Y_2O_3 stabilized tetragonal zirconia (ZrO_2) polycrystalline) balls of 5 mm diameter as the milling media, to reduce particle size and achieve homogenous mixing. The powders of pure ZrB_2 phase and the ZrB_2–SiC composite samples were first uniaxially pressed into disks with an approximate diameter of 25 mm under a pressure of 35 MPa. The pressed disks were then subjected to cold isostatic pressing at 414 MPa for further compaction. The samples were then hot pressed according to conditions detailed in Table 1. While the ZrB_2 samples were hot pressed at 1700 °C for 3 h under 35 MPa of pressure, the ZrB_2–SiC composite samples were hot pressed at 1900 °C for 2 h under 35 MPa pressure. The entire hot pressing was performed in an Ar atmosphere and a heating rate of 50 °C/min was used. The furnace was turned off after holding for the specified time at the targeted temperature. Disks with a diameter of ~25 mm and thickness of

Table 1
Raw materials and processing conditions for preparation of ZrB_2 and ZrB_2–SiC composite samples.

Sample	Composition (vol. %)		Powder preparation		Hot pressing
	ZrB_2	SiC	Ball milling	Drying	Temp./time/pressure
ZrB_2	100	0	None	–	1700 °C/3 h/35 MPa
70:30 ZrB_2–SiC	70	30	24h; 3Y-TZP[a] media	150 °C	1900 °C/2 h/35 MPa
50:50 ZrB_2–SiC	50	50	24h; 3Y-TZP[a] media	150 °C	1900 °C/2 h/35 MPa

[a] 3 mol% Y_2O_3 stabilized tetragonal zirconia (ZrO_2) polycrystals.

~5 mm were produced. Smaller specimens having dimensions of 5 mm × 3 mm × 0.5 mm were cut from the disks by using a slow action diamond saw (Isomet, Buehler Ltd., Evanston, IL, USA) and polished to a 6 μm surface finish. The final samples for microstructure characterization and oxidation studies using TGA, differential scanning calorimetry (DSC), and HTXRD, had dimensions of 5 mm × 3 mm × 0.3 mm.

2.2. Microstructure characterization

The physico-chemical characteristics of the hot pressed samples were determined using a variety of methods. Bulk density, apparent specific gravity and apparent porosity of the hot pressed samples were measured by the Archimedes method, following the procedure detailed in ASTM C20.[38] The samples used for these measurements were semi-circular in shape (diameter ~25 mm, height ~5 mm) and were prepared by sectioning the hot pressed sample disks using the slow action diamond saw, followed by ultrasonic cleaning. All samples were dried at 105 °C for 24 h in air before any measurements were taken. Although the sample sizes used for these measurements were smaller than those recommended in ASTM C20, they were considered adequate for the purpose of this study. Distilled water was used as the suspending medium.

The microstructure and elemental composition of hot pressed and oxidized samples were characterized by scanning electron microscopy (SEM) and energy dispersive spectroscopy (EDS) using a Hitachi S-4700 (Hitachi High Technologies, Schaumburg, IL, USA) and a JEOL JSM-6060LV (JEOL USA, Inc., Peabody, MA, USA) scanning electron microscopes (SEMs). The hot pressed samples of ZrB_2 and ZrB_2–SiC composites used for SEM/EDS analyses had dimensions of 5 mm × 3 mm × 0.3 mm, and were polished to a 1 μm surface finish on Buehler's ECOMET III polisher/grinder (Buehler Ltd., Evanston, IL, USA) using a diamond paste (Buehler METADI Aerosol Spray Diamond Compound—1 Micron; Buehler Ltd., Lake Bluff, IL, USA). The oxidized ZrB_2 and ZrB_2–SiC composite samples were first impregnated with an epoxy resin (Epo-Thin, Buehler Ltd., Lake Bluff, IL, USA), and then sectioned to enable examination of the cross-section. These samples were also polished to a 1 μm surface finish using the diamond paste. Water was used as a lubricant during sectioning and polishing. All SEM samples were mounted on aluminum stubs and sputter coated with ~6 nm of a Au/Pd alloy to facilitate imaging. The samples used for EDS analysis were coated with carbon instead of Au/Pd, and flat sample regions were examined using a 20 kV or 15 kV accelerating voltage and a 10 mm working distance. Copper was used to calibrate the energy and a minimum of six acquisitions were taken on each sample.

The crystalline composition of the hot pressed and oxidized samples was determined by synchrotron X-ray diffraction (XRD). Plate-shaped samples (with dimensions of 5 mm × 3 mm × 0.3 mm) were studied in transmission geometry. Further details on the instrumentation and calibration of the XRD experiments are included in Section 2.3.2. The XRD patterns were subsequently analyzed by the Rietveld method[39] using the JADE software (Materials Data, Inc., Livermore, CA, USA) to determine the crystalline phase composition as well as crystallographic parameters for each constituent phase.

2.3. Oxidation studies

The oxidation of ZrB_2 and ZrB_2–SiC composites was studied using TGA/DSC and HTXRD. The samples used for these studies were hot pressed plates (5 mm × 3 mm × 0.3 mm) which had been polished to a 6 μm surface finish.

2.3.1. TGA/DSC studies

Simultaneous TGA and DSC studies were conducted on hot pressed ZrB_2 and ZrB_2–SiC composites. Samples were heated at 10 °C/min in a Netzsch DSC/TGA (Model STA409 CD™, Export, PA, USA) instrument. While the ZrB_2 sample was heated up to 1350 °C, the ZrB_2–SiC composite samples were tested up to 1500 °C. An alumina (Al_2O_3) pan fitted with a lid was used to hold the specimen and as a reference. During the analysis, the sample chamber was purged with He (25 mL/min) and air (50 mL/min).

2.3.2. In situ high temperature synchrotron diffraction studies

In a typical HTXRD experiment, the hot pressed plate specimens were heated, and the crystalline composition and structural changes were simultaneously recorded as XRD patterns using synchrotron radiation and a curved image plate (CIP) detector.[36] All experiments were conducted at the 33BM-C beam line at the Advanced Photon Source (APS) at Argonne National Laboratory, Argonne, IL, USA. The experimental set-up used for these studies is shown in Fig. 1. Plate samples were mounted vertically, perpendicular to the incident X-ray beam, in a specially designed sample holder made with Pt–20%Rh and heated using a quadrupole lamp furnace (QLF).[35] The schematic of the sample holder along with the specimen is shown in Fig. 2. The sample was coated with Pt powder (0.15–0.45 μm, 99.999% pure, Aldrich, Milwaukee, WI, USA) on the side facing the incident X-ray beam and was used to determine sample temperature from the expansion of the Pt lattice. The QLF is a radiation heating furnace that can be used to conduct HTXRD investigations of ceramics in air up to 2000 °C in air.[32–35] The details of the construction, operation and capabilities of the CIP detector, used in these studies, are reported elsewhere.[36] The CIP detector allows for simultaneous acquisition of diffracted X-ray intensities over a 2θ range extending from 2° to 35°, thus eliminating any time dependence in XRD pattern acquisition. Contingent upon sample properties and incident X-ray beam intensity, high resolution XRD patterns can be acquired in ≤20 s using this detector.[37] For the purpose of this study, the CIP detector was first aligned and calibrated using a Si(1 1 1) analyzer crystal and the LaB_6 powder standard (SRM 660a, National Institute of Standards and Technology, Gaithersburg, MD, USA). Incident monochromatic X-rays of wavelength 0.70087 Å, as calibrated with SRM 660a, were used in this work.

Oxidation of ZrB_2 was studied by heating the plate sample in air to discreet set temperatures (T_{set}) in steps of ~100 °C, from room temperature up to ~1500 °C, and X-ray diffraction

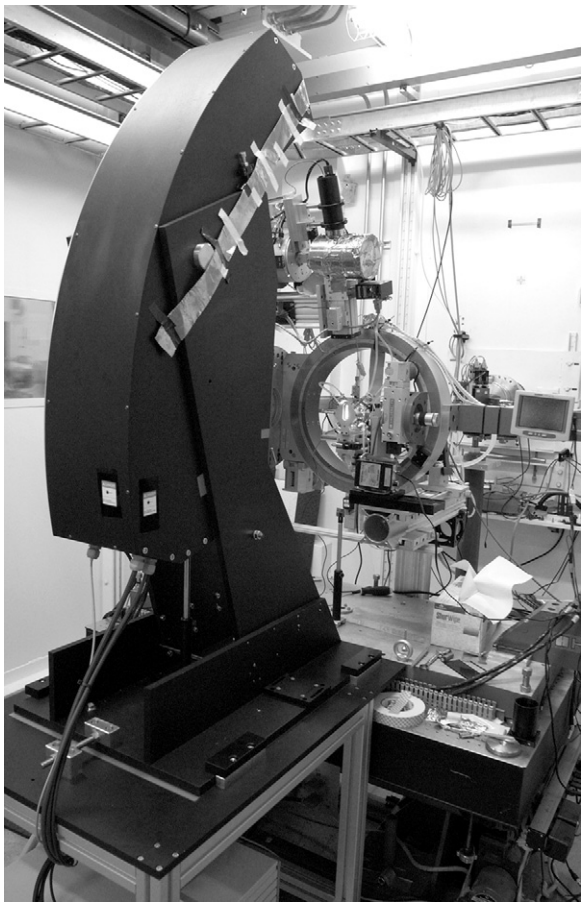

Fig. 1. Photograph of the HTXRD experiment set-up at the 33BM-C beam line at APS, Argonne National Laboratory. A curved image plate (CIP) detector was used with a quadrupole lamp furnace (QLF).

patterns were acquired in situ, in transmission geometry at each temperature step. At least four HTXRD patterns were collected and averaged at each temperature, to improve signal-to-noise ratio. The sample temperature (T_{sample}), which is different from the set temperature (T_{set}) when using the QLF,[35] was determined later during analysis of HTXRD patterns from the lattice expansion of cubic Pt. In order to maximize random orientation of the crystallites, the plate samples were rocked ±1° about a horizontal axis perpendicular to the incident X-ray beam. The sample was cooled down to room temperature after the highest temperature run (i.e. T_{set} = 1500 °C) in ∼5 min and XRD patterns were recorded to determine the final crystalline phase composition after oxidation.

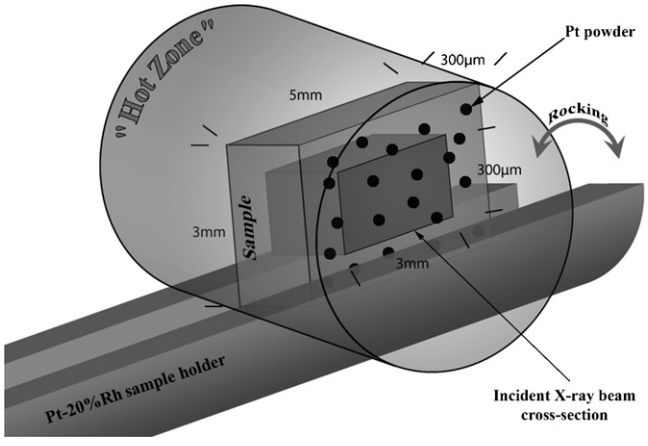

Fig. 2. Schematic of the sample holder used to mount hot pressed plate samples for HTXRD studies in transmission geometry.

Isothermal HTXRD studies were conducted in air in order to evaluate the effect of SiC on the oxidation of ZrB_2. Plate samples of ZrB_2 and ZrB_2–SiC composites were heated to T_{set} = 1100 °C in ∼5 minutes, and several HTXRD patterns were acquired over the next ∼1 h duration while the samples were maintained at the T_{set} temperature. Based on prior experience and the location of the control thermocouple (which measures T_{set}) in the QLF, the sample temperature (T_{sample}) during these studies was expected to be in the range 1200–1350 °C.[32–35,37] This temperature was selected for the isothermal studies as it corresponded to oxidizing conditions in a partial protective regime for the materials being evaluated. Therefore, it was anticipated that a pronounced effect of the presence of SiC on oxidation of ZrB_2 could be suitably observed. Following the isothermal studies, each sample was cooled down to room temperature in ∼5 min. XRD patterns were also collected at room temperatures for the ZrB_2 and ZrB_2–SiC composite samples, both before and after the isothermal studies, to determine the initial and final crystalline phase composition.

All the XRD patterns, including those acquired at room temperatures and at high temperatures, were analyzed by the Rietveld method using the JADE software (Materials Data, Inc., Livermore, CA, USA) to extract the quantitative crystalline phase composition and crystallographic parameters. The PDF-4 2008 database from ICDD (International Center for Diffraction Data, Newtown Square, PA, USA) and the Inorganic Crystal Structure Database (NIST, Gaithersburg, MD, USA; and Fachinformationszentrum (FIZ), Karlsruhe, Germany) were used for crystalline phase identification. The structure parameters of the crystalline phases identified from the databases were used as starting parameters during refinement. Besides the lattice constants for each phase, other factors that were refined included scaling factors, sample displacement, profile function parameters, and isotropic temperature factors (where possible).

3. Results and discussion

3.1. Microstructure of processed samples

The microstructure of the hot pressed ZrB_2 and the ZrB_2–SiC composites was fairly porous as is evident from the SEM micrographs presented in Fig. 3. In the case of the 70:30 ZrB_2–SiC and the 50:50 ZrB_2–SiC samples, SiC was fairly uniformly distributed in the ZrB_2 matrix (see inset in Fig. 3(b) and (c)). The grain size of the ZrB_2 phase was larger in the pure ZrB_2 specimen (Fig. 3(a)) in comparison to the composite samples. This is most likely due to the presence of SiC which can act as a grain growth inhibitor. Moreover, the latter samples had also been subjected to 24 h of ball milling during sample processing. The crystalline phase composition of each of the samples was

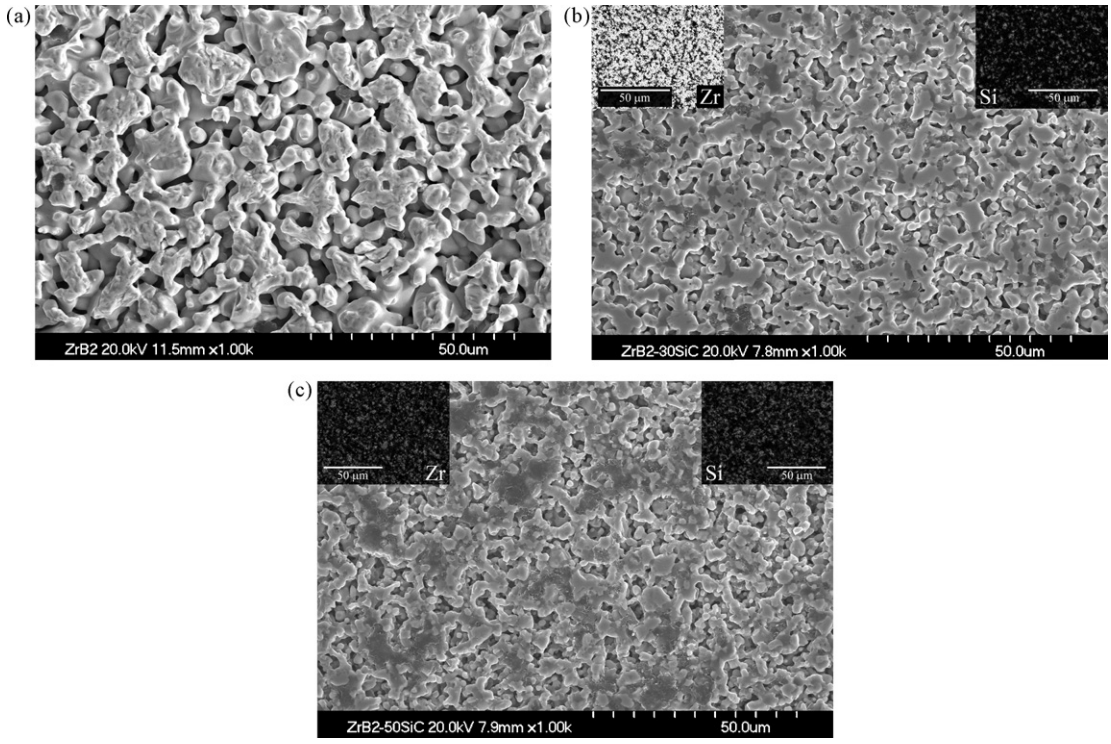

Fig. 3. SEM micrographs of the processed samples: (a) ZrB_2, (b) 70:30 ZrB_2–SiC, and (c) 50:50 ZrB_2–SiC. Elemental maps of Zr and Si are shown as insets for 70:30 ZrB_2–SiC and 50:50 ZrB_2–SiC samples.

verified by Rietveld analysis of the XRD patterns collected at room temperature for each sample. The results are included in Table 2 and they confirmed that the hot pressed composite samples had the component phases in the desired proportion. There was no evidence of any impurities or of the formation of any oxidized crystalline phases during sample processing.

The density and porosity of the hot pressed samples, measured using the Archimedes' method, were consistent with the observed microstructures (see Table 2). While the pure ZrB_2 and the 50:50 ZrB_2–SiC samples had >30% porosity, the 70:30 ZrB_2–SiC composite samples were 23.7% porous. The measured apparent densities of the composite samples were consistent with the expected values calculated using densities of each component phase and the phase composition. Therefore, it was concluded that porosity in the composite samples was predominantly interconnected. However, considerably low apparent density value of the pure ZrB_2 sample, in comparison to pure ZrB_2 phase, suggests the presence of closed pores. Since this study was aimed at examining the oxidation behavior of hot pressed ZrB_2 and ZrB_2–SiC, samples with interconnected porosity were considered particularly suitable to measure oxidation kinetics in reasonable time due to the increased surface area available for oxidation. This argument is especially relevant for HTXRD studies using synchrotron radiation, as experimental time is limited.

3.2. Oxidation studies using TGA/DSC

Percentage weight changes *vs.* temperature of the ZrB_2 and the ZrB_2–SiC composites during non-isothermal heating up to 1500 °C are presented in Fig. 4(a). The heating rate of 10 °C/min allowed for detection of suitable DSC signal to assess any exothermic or endothermic processes occurring during oxidation. No change in the samples was observed up to ~650 °C, which was followed by a rapid increase in mass due to oxidation. This was also detected as an exothermic event in the DSC signal. The onset of oxidation was delayed in the ZrB_2–SiC samples, and T_{start} of 661, 670, and 691 °C were recorded for the pure ZrB_2, 70:30 ZrB_2–SiC and the 50:50 ZrB_2–SiC samples, respectively. The delay in the onset of oxidation of ZrB_2 in the

Table 2
Physical properties and crystalline phase composition of hot pressed ZrB_2 and ZrB_2–SiC composite samples.

Sample	Density (g/cm^3)		Total porosity (vol. %)	Crystalline phase composition from XRD			
	ρ_{bulk}	$\rho_{apparent}$		Weight %		Volume %	
				ZrB_2	SiC	ZrB_2	SiC
ZrB_2	3.84	5.68	32.3	100	0	100	0
70:30 ZrB_2–SiC	4.07	5.34	23.7	82.6 ± 0.7	17.4 ± 0.4	71.5 ± 0.3	28.5 ± 0.1
50:50 ZrB_2–SiC	2.96	4.63	35.9	67.4 ± 0.4	32.6 ± 0.3	52.3 ± 0.1	47.7 ± 0.1

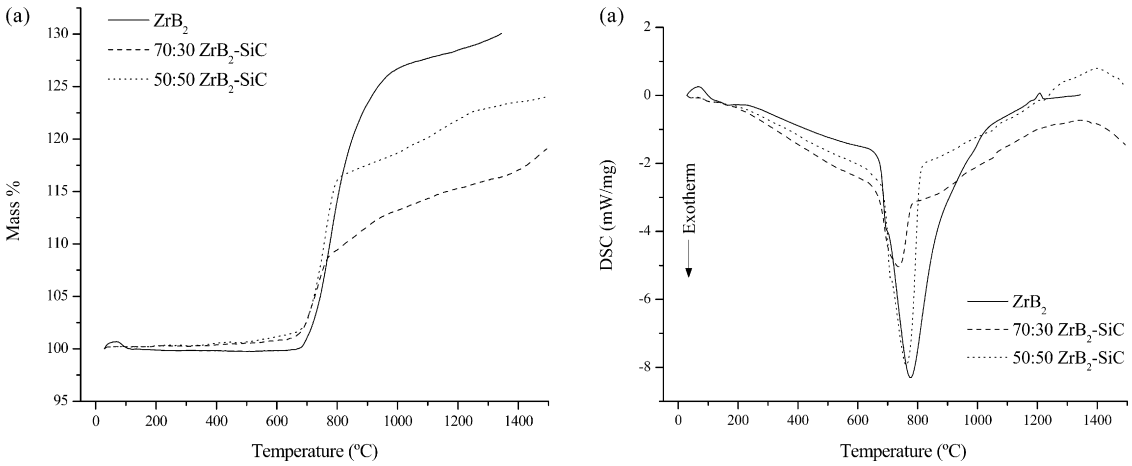

Fig. 4. Thermal analysis studies on ZrB_2 and ZrB_2–SiC composite samples, from 20 to 1450 °C in air: (a) TGA and (b) DSC.

ZrB_2–SiC composites is most likely due to coating of the ZrB_2 grains with SiC, as seen in the SEM micrographs (Fig. 3(b) and (c)). The rapid increase in weight observed in all the samples between 700 and 800 °C is consistent with the high porosity and larger surface area, which ensured the availability of the ZrB_2 phase for active oxidation. The 50:50 ZrB_2–SiC samples were more porous than the 70:30 ZrB_2–SiC samples (see Table 2). The overall weight gain observed in the 50:50 ZrB_2–SiC sample, in the studied temperature range, was larger than the 70:30 ZrB_2–SiC sample. This could be a result of higher SiC content in the sample. It is reasonable that in the investigated temperature range the net gain in weight in the 50:50 ZrB_2–SiC composite sample is primarily determined by the oxidation of SiC. This can be comprehended better by considering complete oxidation of ZrB_2 to ZrO_2 and SiC to SiO_2 in the samples, along with the loss of B_2O_3 due to vaporization. With this assumption, the final increase in weight for the pure ZrB_2 sample, the 70:30 and the 50:50 ZrB_2–SiC composites is expected to be 9.2%, 16.6% and 22.3%, respectively. In this case, the weight gain in both the composite samples is dominated by the oxidation of SiC, and is calculated as ∼9% (of the 16.6%) for the 70:30 ZrB_2–SiC sample and ∼16% (of the 22.3%) for the 50:50 ZrB_2–SiC sample. The loss of Si as SiO species is assumed to be negligible in this argument.

Based on these TGA/DSC studies alone, it is difficult to judge the efficacy of SiC content in protecting ZrB_2 from oxidation. The change in slopes of the TGA curves at around 800 °C in the composite samples, and again at ∼900 °C, suggest a slower rate of oxidation which is perhaps due to the transient oxidation protection afforded by the liquid B_2O_3 phase. Beyond ∼1200 °C, the increase in slope of the TGA curves for the pure ZrB_2 and the 70:30 ZrB_2–SiC samples suggest rapid oxidation due to vaporization of B_2O_3 phase. On the other hand, the decrease in the rate of weight gain observed in the 50:50 ZrB_2 sample is most likely due to formation of a glassy SiO_2 layer which protects rapid oxidation of the underlying ZrB_2 phase. The DSC data is unremarkable except for the large exothermic peaks due to oxidation reactions. The presence of a small endothermic peak at ∼1200 °C, observed only in the case of the pure ZrB_2 sample, does suggest a possible transformation of the monoclinic ZrO_2 (m-ZrO_2) phase, expected to be formed on oxidation of ZrB_2, to tetragonal ZrO_2 (t-ZrO_2) phase.[40,41]

3.3. Oxidation of ZrB_2—crystalline phase evolution with temperature

The evolution of crystalline phases during oxidation of pure ZrB_2 sample in air was recorded as a series of HTXRD patterns in discreet T_{set} steps of 100 °C, from room temperature to T_{set} = 1500 °C in air. Although HTXRD datasets were collected over a 2θ range from 2° to 35°, only segments of the dataset are presented in Fig. 5 for clarity. Each HTXRD pattern presented in Fig. 5 was averaged over 4 different exposures which were recorded in ≤4 min total time, while the sample was maintained at the specified T_{set}. The set temperature was increased in steps of 100 °C in 1 min, followed by equilibration for 1 min before acquisition of 4 different exposures using the CIP detector. Based on lattice expansion of the Pt phase, which was coated on one side of the sample, the oxidation behavior of ZrB_2 was studied in the temperature range extending from 20 to 1627 °C in air.

Qualitative changes occurring during oxidation of ZrB_2 are clearly evident from the HTXRD patterns in Fig. 5. The drift of the diffraction peaks for all the phases towards lower 2θ angles, is the result of temperature induced expansion of crystal lattices of each phase. The change in the Pt peak around 29°, starting as a broad peak at 20 °C to a well defined sharp peak, is a result of Pt crystallite growth with increase in temperature. The first crystalline oxide phase as a result of ZrB_2 oxidation was found to be t-ZrO_2 (ICDD PDF#04-005-4504). Subsequent appearance and disappearance of the m-ZrO_2 (ICDD PDF # 01-083-0936) peaks due to transformation into t-ZrO_2 phase at higher temperatures ($T_{sample} \geq 1250$ °C) was also observed. Although not apparent from the HTXRD patterns in Fig. 5, a broad peak, symbolic of the presence of an amorphous phase, was observed in patterns acquired at $T_{sample} \geq 935$ °C (or $T_{set} \geq 700$ °C).

The analysis of the HTXRD patterns using the Rietveld method provides a quantitative insight into the oxidation of ZrB_2 at high temperatures. The results are presented in Fig. 6 as weight percentage composition of crystalline phases observed

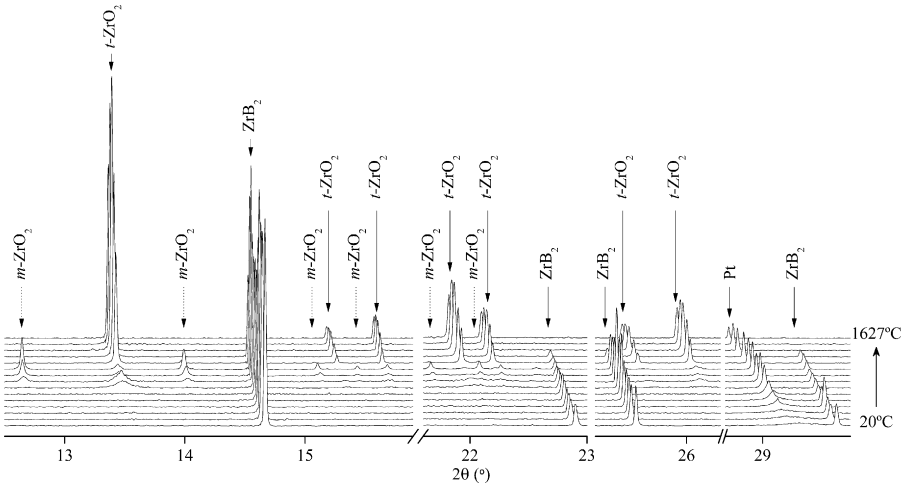

Fig. 5. High temperature XRD study of ZrB_2, from 20 to 1627 °C, in air.

at each temperature. The smooth lines drawn through the data points are merely a guide to assist in clearer depiction of the results and should not be misconstrued to represent composition at intermediate temperatures between any two measured data points. No oxidation of ZrB_2 was observed up to 800 ± 3 °C, beyond which the ZrB_2 content of the sample decreased continuously, resulting in the formation of t-ZrO_2 or m-ZrO_2 phases. As stated above, the first oxidized phase to be observed was t-ZrO_2 which appeared as broad peaks, most notably around 13.5°, at 906 ± 1 °C. The overall composition at this temperature was $81.7 \pm 0.5\%$ ZrB_2 (ICDD PDF # 04-004-7151) and $18.3 \pm 0.3\%$ t-ZrO_2 by weight. Upon heating to 997 ± 1 °C the m-ZrO_2 phase was formed and its concentration increased from $13.1 \pm 0.3\%$ to $33.8 \pm 0.3\%$ (weight %) at 1169 ± 1 °C, while the t-ZrO_2 content decreased from $18.8 \pm 0.2\%$ to $4.2 \pm 0.1\%$ (weight %) in the same temperature range. Heating the sample to higher temperatures resulted in complete conversion of m-ZrO_2 to t-ZrO_2 by 1250 ± 1 °C, and only t-ZrO_2 phase was observed at higher temperatures. The ZrB_2 phase in the sample was completely oxidized by 1477 ± 1 °C.

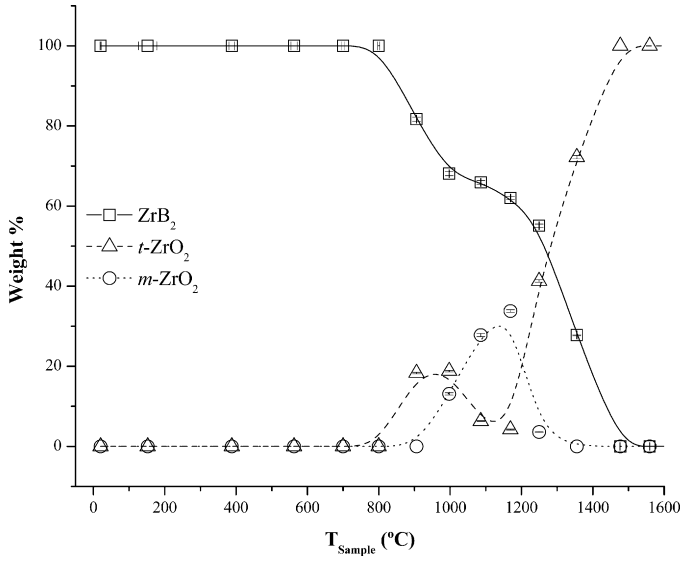

Fig. 6. Crystalline phase evolution with temperature during oxidation of ZrB_2 in air.

The observation of t-ZrO_2 at temperatures below the transformation temperature (i.e. 1170 °C) is most likely due to the particle size effect, which has been previously reported.[40,41] A reasonable estimate of the average crystallite size, or coherently scattering crystalline domains, can be made from the broadening of diffraction peaks, which is attributable only to the sample. In the case of ceramic phases, crystallite sizes are often similar to grain sizes. The average crystallite size of t-ZrO_2 was calculated to be 19 nm at 906 ± 1 °C, which increased to 73 nm at 1169 ± 1 °C. This estimation was made after taking into account the instrumental broadening, which was determined using SRM 660a LaB_6 powder. Since this calculation made use of the Scherrer formula,[42] any microstrains present were ignored, and the crystallite size values may be underestimated. Nonetheless, crystallite size measurements are consistent with the presence of t-ZrO_2 phase at lower temperatures than expected. The presence of m-ZrO_2 phase up to 1250 ± 1 °C, even though only in small amounts (i.e. $3.6 \pm 0.1\%$ by weight), is intriguing. It is expected that all the m-ZrO_2 phase transforms to t-ZrO_2 phase by 1170 °C.[40,41] However, it is possible that due to impurities such as Hf in the starting ZrB_2 phase, this anomaly was observed. It is also conceivable that due to slow diffusion of oxygen through a liquid B_2O_3 layer a defect m-ZrO_2 structure is formed with oxygen vacancies resulting in its stability up to higher temperatures. Overall, non-isothermal HTXRD studies were quite similar to the TGA/DSC studies reported in Section 3.2, but provided clearer and quantitative insight into oxidation of ZrB_2, and the formation and transformations of the crystalline oxidized phases.

3.4. Isothermal oxidation studies

Isothermal oxidation studies of ZrB_2 and ZrB_2–SiC composites using HTXRD were conducted in order to (a) evaluate the usefulness of the method towards understanding oxidation kinetics of UHTC diborides by monitoring changes in the crystalline phase composition and (b) to examine the effect of SiC on

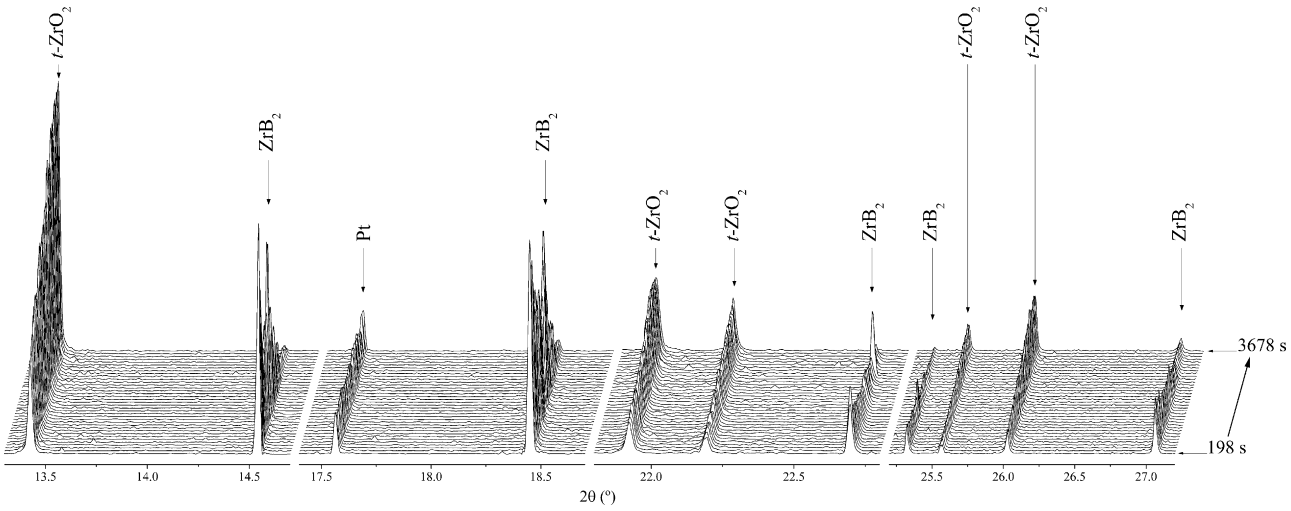

Fig. 7. Isothermal high temperature XRD study of ZrB_2 at 1268 ± 3 °C in air.

the oxidation kinetics of ZrB_2 in ZrB_2–SiC composite ceramics. Once again, the sample temperature was determined from the lattice expansion of Pt. Fig. 7 shows the series of HTXRD patterns that were collected at 1268 ± 3 °C to observe oxidation of pure ZrB_2. Each of the thirty-seven HTXRD patterns presented in Fig. 7 was recorded using the CIP detector in approximately 1 min 41 s, while the sample was maintained at the specified temperature. The first HTXRD pattern was collected after the sample had been heated at 1268 ± 3 °C for 198 s, while the last HTXRD pattern at this temperature was recorded 3678 s after reaching the temperature. The sample was exposed to the X-ray beam for 30 seconds for each HTXRD pattern. Only segments of the dataset are presented, although HTXRD datasets were collected over a 2θ range from 2° to 35°. Each subsequent HTXRD pattern has been offset, both along the vertical direction as well as to the right along the 2θ axis, to clearly show the growing and the diminishing crystalline phase peaks belonging to *t*-ZrO_2 and the ZrB_2 phases, respectively. No change was observed in the Pt peak location or intensity during the entire experiment. The ZrB_2 peak intensities gradually decreased with time of exposure to high temperature, while the *t*-ZrO_2 phase peaks consistently increased in intensity. Occasionally, a few peaks for ZrB_2 phase defied the trend and have higher intensity than observed in the preceding patterns, for example the peaks near 14.5°, 18.5° and 22.6°. This is most likely due to transient preferred orientation recorded during the 30 s exposure to X-ray beam, and is due to the inability to achieve completely random orientation of the diffracting ZrB_2 crystallites by rocking ± 1°. After 3678 s at 1268 ± 3 °C, the sample was cooled to room temperature in <10 min, and XRD patterns confirmed that ZrB_2 phase had been completely oxidized and *m*-ZrO_2 was the only crystalline phase present.

Similar isothermal studies were also conducted for the ZrB_2–SiC composite samples, although at different temperatures and for different durations of times. Each HTXRD pattern was recorded using a 30 s exposure of the sample to the X-ray beam. In the case of 70:30 ZrB_2–SiC sample fifty-two HTXRD patterns were collected with a time resolution of 1 min 16 s at 1276 ± 3 °C, while forty-seven HTXRD patterns were collected with a time resolution of 1 min 27 s for the 50:50 ZrB_2–SiC sample at 1334 ± 2 °C. After collecting HTXRD patterns for 3847 s and 3776 s for the 70:30 ZrB_2–SiC and the 50:50 ZrB_2–SiC samples, respectively, the samples were cooled to room temperature in <10 min, and XRD patterns were recorded to ascertain the final crystalline phase compositions after oxidation. Using the Rietveld method, the final compositions of the oxidized 70:30 ZrB_2–SiC sample expressed in weight % was 42.7 ± 0.7% ZrB_2, 12.4 ± 0.5% SiC (ICDD PDF # 01-074-2307), 41.6 ± 0.9% *m*-ZrO_2 and 3.3 ± 0.2% *t*-ZrO_2. The oxidized 50:50 ZrB_2–SiC sample was comprised of 34.1 ± 0.4% ZrB_2, 24.9 ± 0.5% SiC, 36.8 ± 0.6% *m*-ZrO_2 and 4.1 ± 0.1% *t*-ZrO_2 by weight. The *t*-ZrO_2 phase found in both the composite samples after cooling was in contrast to the pure ZrB_2 sample. It is believed that most of the *t*-ZrO_2 phase formed at higher temperatures would have achieved significant crystallite coarsening and would transform to *m*-ZrO_2 upon cooling. However, both the composite samples also had ZrB_2 phase remaining at the end of the isothermal study, which could have oxidized during cooling to produce small crystallites of *t*-ZrO_2 which remained stable at room temperature. This is consistent with the appearance of *t*-ZrO_2 phase as the first oxidized crystalline phase observed during the non-isothermal studies on ZrB_2 reported in Section 3.3. In addition, a boron carbide phase ($B_{13}C_2$, ICDD PDF # 04-002-9582) was also present as a minor phase in both the cooled composite samples, but this phase was excluded from the final quantitative analysis. The boron carbide phase was not observed in any of the XRD patterns which were acquired at high temperatures. Therefore, it is believed that it may have been formed as a result of rapid cooling of a microstructure which comprised of B_2O_3 liquid phase in the presence of the SiC phase. Further investigation of this observation was not pursued as it was considered beyond the scope of the current work.

The post-oxidation microstructures of the ZrB_2 and the ZrB_2–SiC composites after the isothermal studies is presented in Fig. 8. The pure ZrB_2 sample was completely oxidized and the resultant microstructure was porous throughout (Fig. 8a). The

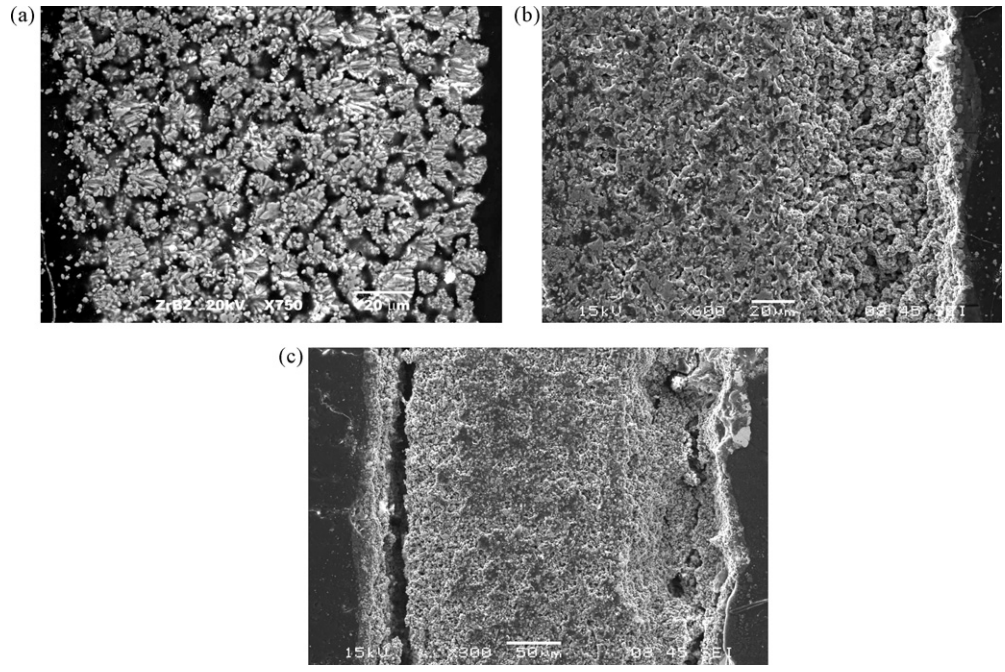

Fig. 8. SEM micrographs of the cross-section of the isothermally oxidized samples: (a) ZrB_2, (b) 70:30 ZrB_2–SiC, and (c) 50:50 ZrB_2–SiC. Please note: the pure diboride sample (ZrB_2) was oxidized at 1268 ± 3 °C for 3678 s; the 70:30 ZrB_2–SiC sample was oxidized at 1276 ± 3 °C for 3847 s; and the 50:50 ZrB_2–SiC sample was oxidized at 1334 ± 2 °C for 3776 s. All the samples were cooled to room temperature after the completion of the isothermal studies in <10 min.

non-oxidized ZrB_2 sample was already porous, and conversion of ZrB_2 to *m*-ZrO_2 phase upon oxidation is associated with a further increase of 14.74% in molar volume. The presence of elongated grains of *m*-ZrO_2 phase was a characteristic feature of the final microstructure suggesting preferential grain growth along certain directions in the ZrO_2 phase. The microstructure of the oxidized 70:30 ZrB_2–SiC and the 50:50 ZrB_2–SiC samples (Fig. 8(b) and (c)) was multilayered. A thin and glassy, Si-rich outside surface layer covered a porous inner layer which was formed above the underlying ZrB_2–SiC composite. There was no indication of elongated grain growth in the porous layer of the composite samples, and it was mainly comprised of the ZrO_2 phase, as verified by elemental analysis using EDS. Both the oxidized 70:30 ZrB_2–SiC and the 50:50 ZrB_2–SiC samples showed the presence of cracks in the porous layer which could be delamination due to thermal expansion mismatch between the surface layer, the porous oxidized layer, and the underlying ZrB_2–SiC matrix. No cracking was observed in the pure ZrB_2 sample after oxidation.

3.5. Effect of SiC addition on oxidation of ZrB_2 in ZrB_2–SiC composites

The effect of SiC addition on the oxidation of ZrB_2 in ZrB_2–SiC composites can be gauged quantitatively by following the crystalline phase evolution during high temperature isothermal studies. ZrB_2, *t*-ZrO_2 and Pt, were the only crystalline phases present in the pure ZrB_2 sample, while SiC was the additional crystalline phase observed in the ZrB_2–SiC composite samples throughout the isothermal study at high temperatures. Results from Rietveld analysis of selected isothermal HTXRD patterns of the samples are presented in Fig. 9. The normalized

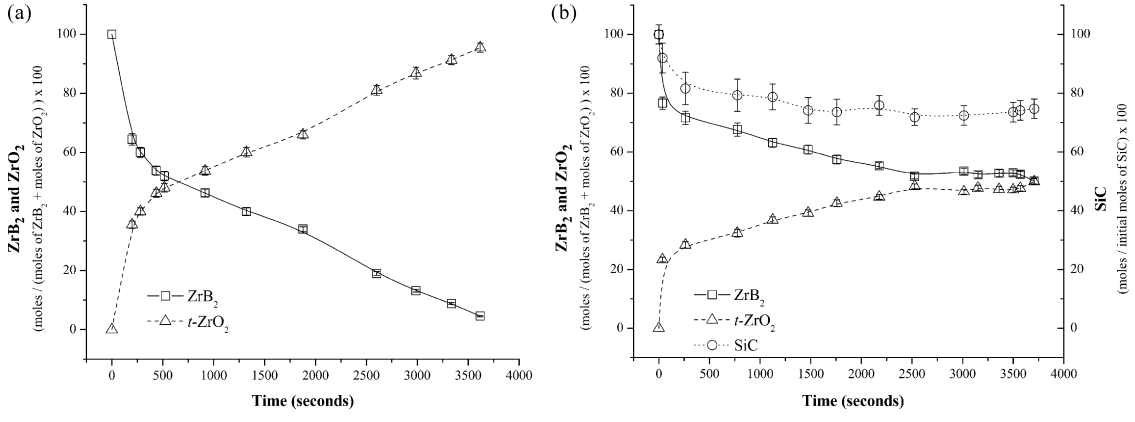

Fig. 9. Crystalline phase changes with time during oxidation of (a) ZrB_2 in air at 1268 ± 3 °C, (b) 70:30 ZrB_2–SiC in air at 1276 ± 3 °C, and (c) 50:50 ZrB_2–SiC in air at 1334 ± 2 °C.

molar concentrations of ZrB_2 and *t*-ZrO_2 are presented on the *y*-axis on the left, while the SiC concentration, normalized by the SiC content in the non-oxidized sample, is plotted on a second *y*-axis on the right for the ZrB_2–SiC composite samples. Using the QLF the samples were heated to the desired temperature in ~5 min and the HTXRD pattern acquisition using the CIP detector was immediately started. The first HTXRD pattern was acquired with a delay as small as 35 s (for the 70:30 ZrB_2–SiC sample) and no larger than 198 s (for the pure ZrB_2 sample) from the time the sample(s) had reached the desired temperature(s). Despite of the high porosity in the samples, a parabolic region in the oxidation of ZrB_2 was observed for all the samples over the first ~500 s, and subsequently, a linear oxidation trend was observed. The slope of the ZrB_2 (or *t*-ZrO_2) curves in the linear region represents the rate of oxidation of the ZrB_2 phase. The SiC content in the 70:30 ZrB_2–SiC and the 50:50 ZrB_2–SiC samples decreased slowly, and approximately 25% of the SiC phase had oxidized in both the samples in ~1 h. The larger error bars for SiC content in the 70:30 ZrB_2–SiC sample are due to higher noise in the HTXRD datasets collected for this sample. Based on this analysis it can be qualitatively seen that the oxidation rate of the ZrB_2 decreased with increasing SiC content in the samples. Since the samples had different initial porosities, and the isothermal runs for each of the samples reported in this study were conducted at different temperatures, a rigorous comparison of the rate of oxidation of ZrB_2 was not possible. It should however be noted that a higher slope of the *t*-ZrO_2 content, suggesting a faster rate of oxidation, was observed in the linear region between 500 and 3000 s for the 70:30 ZrB_2–SiC than for the 50:50 ZrB_2–SiC. Not only did the 70:30 ZrB_2–SiC have the least porosity and the 50:50 ZrB_2–SiC have the highest porosity of all the samples investigated as part of this study, the isothermal study for 50:50 ZrB_2–SiC was also conducted at a markedly higher temperature ($1334 \pm 2\,^{\circ}C$). These observations raise some relevant questions regarding the factors that can influence oxidation kinetics in the experimented temperature range. The oxidation protection offered by the silica layer in the examined temperature range in a rigid but porous sample, along with the role of microstructure and porosity in facilitating the formation of the silica layer, certainly deserve some consideration. Perhaps, it could be interesting to explore oxidation behavior of a ZrB_2–SiC composite which has a thin layer of SiC on the outside surface.

The fractional conversion of ZrB_2 to ZrO_2 in the studied UHTC diborides, as determined using HTXRD, can also be used to estimate the thickness of the oxidation layer as it is formed. The HTXRD experiments in transmission mode examined a volume element of the sample which extended through the sample and had two surfaces exposed to air with an area 'A', determined by the X-ray beam cross-section (see Fig. 2). The fraction of the ZrB_2 phase which is converted to *t*-ZrO_2, therefore, is equivalent to the ratio of the volume of the oxide layer (formed on both exposed surfaces) to the total sampled volume. The final expression for oxide layer thickness, denoted by 'Δt' and presented in Eq. (2), takes into consideration the fraction of the sample which is porous '*p*' at the onset of the experiment, the initial volume fraction of ZrB_2 (V_{ZrB_2}), and the fractional increase in volume

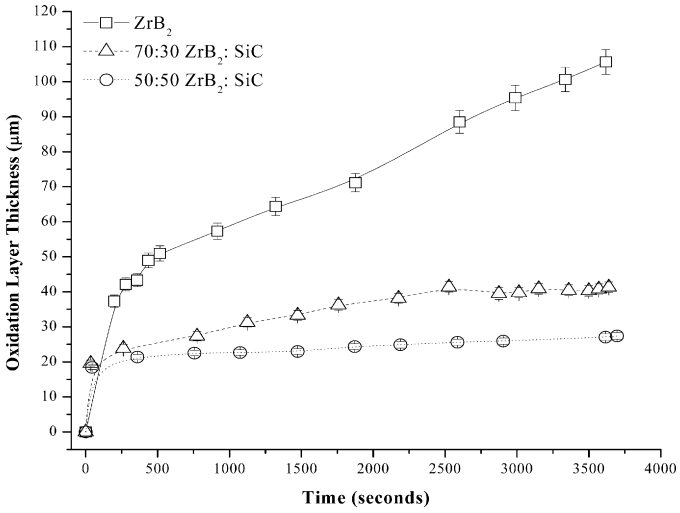

Fig. 10. Change in thickness of the oxidation layer formed with time in pure ZrB_2 and ZrB_2–SiC composite samples during isothermal studies at temperatures ≥1250 °C.

due to conversion of ZrB_2 to *t*-ZrO_2 ($\Delta v_{ZrB_2 \rightarrow t\text{-}ZrO_2}$):

$$\Delta t = \frac{x \times t \times A \times V_{ZrB_2} \times (1 - p) \times (1 + (x \times \Delta v_{ZrB_2 \rightarrow t\text{-}ZrO_2}))}{2 \times A} \quad (2)$$

In the above expression '*x*' is the molar fraction of ZrB_2 converted to *t*-ZrO_2, which is determined using the HTXRD, and '*t*' is the thickness of the non-oxidized sample. Any changes in porosity in the sample during oxidation or the contribution of the thin glassy silica surface layer to the oxidation layer thickness are also ignored. An inherent assumption in the derivation of this expression is the movement of the oxidation front into the specimen, parallel to the surface of the specimen. While this may be expected for dense, bulk diboride samples, it can be modified by the presence of porosity, and in particular interconnected porosity in the sample microstructure.

Despite of these simplifications, the derived expression can provide a reasonable estimate of the average thickness of the oxidized layer being formed during oxidation especially in dense diboride samples. The effect of SiC on the oxidation layer thickness, formed due to oxidation of ZrB_2 to *t*-ZrO_2, is shown in Fig. 10. The results from pure ZrB_2 are also included for comparison. Notwithstanding the differences in the physical microstructures of the starting samples, and the differences in temperatures that were used for the isothermal HTXRD runs for each of the samples, it can be seen that increasing the SiC content decreased the rate of oxidation of ZrB_2. The oxide layer thickness determined using this approach should be further adjusted for the increase in volume associated with *t*-ZrO_2 to *m*-ZrO_2 conversion on cooling to room temperature ($\Delta v \sim 4.84\%$), in order to compare the calculated results with the layer thickness determined by ex situ SEM imaging. The thickness of the oxidation layer formed and observed using the SEM (shown in Fig. 8), correlates well with the calculated values (shown in Fig. 10). It is important to acknowledge that this comparison was undertaken merely as an exercise and not as a rigorous proof of the

concept. However, it still presents a novel alternative to estimate the oxidation layer thickness as it is formed during oxidation of ZrB_2 and ZrB_2–SiC ceramics, especially for dense samples, as a function of time and temperature with reasonable accuracy.

4. Summary

High temperature X-ray diffraction was successfully used to examine the oxidation of ZrB_2 in situ, at high temperatures in air, in pure ZrB_2 and ZrB_2–SiC composite ceramics. Increasing the SiC content in the ZrB_2–SiC composites retarded the oxidation of ZrB_2. Both non-isothermal and isothermal HTXRD studies on the UHTC diboride samples were possible due to the improved X-ray detector system and the QLF, which allowed rapid heating of samples in air up to high temperatures (up to 2000 °C). HTXRD methods provide useful information, complementary to the conventional TGA/DSC methods, when used to study the oxidation of diboride ceramics. It was possible to identify and quantify any intermediate crystalline phases that were formed during oxidation of ZrB_2, in real time. The presence of concurrent phases, amorphous or crystalline, or simultaneous reactions, were not limiting and the oxidation of ZrB_2 phase could be followed independently. In addition, a novel approach to estimate the thickness of oxidation layer formed during oxidation of ZrB_2 and ZrB_2–SiC composites, in situ at high temperatures, has been proposed. It is based on fractional conversion of ZrB_2 to ZrO_2, as determined using HTXRD, and perhaps will be most appropriate for application to oxidation of dense ZrB_2 and ZrB_2–SiC composites.

Development of UHTC materials can benefit immensely from HTXRD studies. It is anticipated that through such investigations, improved insight will be gained into the effect of sample microstructure and composition on ZrB_2 oxidation. This can guide the development of improved models to predict the lifetime and performance of UHTCs under operational conditions.

Acknowledgments

P. Sarin and R. P. Haggerty were supported by the AFOSR FA9550-06-1-0386; P.E. Driemeyer and J.L. Bell were supported by the AFOSR FA9550-06-1-0221; and Z.D. Apostolov was supported by the SMART Scholarship by the Department of Defense. The CIP detector was designed and built under an AFOSR DURIP award number FA9550-04-1-0345. The Advanced Photon Source, Argonne National Laboratory is supported by the US DOE, BES-Materials Sciences, under Contract No: W-31-109-ENG-38.

References

1. Opeka MM, Talmy IG, Zaykoski JA. Oxidation-based materials selection for 2000 °C + hypersonic aerosurfaces: theoretical considerations and historical experience. *Journal of Materials Science* 2004;**39**(19): 5887–904.
2. Monteverde F, Bellosi A, Guicciardi S. Processing and properties of zirconium diboride-based composites. *Journal of the European Ceramic Society* 2002;**22**(3):279–88.
3. Van Wie DM, Drewry Jr DG, King DE, Hudson CM. The hypersonic environment: required operating conditions and design challenges. *Journal of Materials Science* 2004;**39**(19):5915–24.
4. White ME, Price WR. Affordable hypersonic missiles for long-range precision strike. *Johns Hopkins APL Technical Digest (Applied Physics Laboratory)* 1999;**20**(3):415–23.
5. Jackson TA, Eklund DR, Fink AJ. High speed propulsion: performance advantage of advanced materials. *Journal of Materials Science* 2004;**39**(19):5905–13.
6. Levine SR, Opila EJ, Halbig MC, Kiser JD, Singh M, Salem JA. Evaluation of ultra-high temperature ceramics for aeropropulsion use. *Journal of the European Ceramic Society* 2002;**22**(14–15):2757–67.
7. Phase diagrams for ceramists—borides, carbides, and nitrides. In: McHale AE, editor. *Phase equilibria diagrams*, vol. 10. Westerville, OH: American Ceramic Society; 1994.
8. Chamberlain AL, Fahrenholtz WG, Hilmas GE, Ellerby DT. High-strength zirconium diboride-based ceramics. *Journal of the American Ceramic Society* 2004;**87**(6):1170–2.
9. Vajeeston P, Ravindran P, Ravi C, Asokamani R. Electronic structure, bonding, and ground state properties of AlB_2-type transition metal diborides. *Physical Review B* 2001;**63**(4).
10. Cutler RA. In: Schneider SJ, editor. *Engineering properties of borides. engineered materials handbook: ceramics and glasses*, vol. 4. Metals Park, OH: ASM International; 1991.
11. Fahrenholtz WG, Hilmas GE, Talmy IG, Zaykoski JA. Refractory diborides of zirconium and hafnium. *Journal of the American Ceramic Society* 2007;**90**(5):1347–64.
12. Pastor H. Metallic borides, preparation of solid bodies-sintering methods and properties of solid bodies. In: Matkovich VI, editor. *Boron and refractory borides*. New York, NY: Springer Verlag; 1977.
13. Kaufman L, Clougherty EV, Berkowitz-Mattuck JB. Oxidation characteristics of hafnium and zirconium diboride. *Transactions of the Metallurgical Society of AIME* 1967;**239**(4):458–66.
14. Berkowitz-Mattuck JB. High-temperature oxidation. *Journal of the Electrochemical Society* 1966;**113**(9):908–14.
15. Irving RJ, Worsley IG. The oxidation of titanium diboride and zirconium diboride at high temperatures. *Journal of the Less Common Metals* 1968;**16**(2):103–12.
16. Kuriakose AK, Margrave JL. The oxidation kinetics of zirconium diboride and zirconium carbide at high temperatures. *Journal of The Electrochemical Society* 1964;**111**(7):827–31.
17. Monteverde F, Bellosi A. Oxidation of ZrB_2-based ceramics in dry air. *Journal of the Electrochemical Society* 2003;**150**(11).
18. Tripp WC, Graham HC. Thermogravimetric study of the oxidation of ZrB_2 in the temperature range of 800 to 1500 °C. *Journal of the Electrochemical Society* 1971;**118**(7):1195–9.
19. Graham HC, Davis HH, Kverens IA, Tripp WC. Microstructural features of oxide scales formed on zirconium diboride materials. In: Kriegel WW, Palmour III H, editors. *Materials science research v. 5. Ceramics in severe environments*, vol. 5. New York, NY: Plenum Press; 1971.
20. Fahrenholtz WG. The ZrB_2 volatility diagram. *Journal of the American Ceramic Society* 2005;**88**(12):3509–12.
21. Chamberlain A, Fahrenholtz WG, Hilmas GE, Ellerby D. Oxidation of ZrB_2–SiC ceramics under atmospheric and reentry conditions. *Refractories Applications Transactions* 2005;**1**(2):2–8.
22. Opeka MM, Talmy IG, Wuchina EJ, Zaykoski JA, Causey SJ. Mechanical, thermal, and oxidation properties of refractory hafnium and zirconium compounds. *Journal of the European Ceramic Society* 1999;**19**(13–14):2405–14.
23. Tripp WC, Davis HH, Graham HC. Effect of an SiC addition on the oxidation of ZrB_2. *American Ceramic Society Bulletin* 1973;**52**(8):612–6.
24. Opila EJ, Halbig MC. Oxidation of ZrB2–SiC. In: Singh M, Jessen T, editors. *25th annual conference on composites, advanced ceramics, materials and structures: A, Ceramic Engineering and Science Proceedings, vol. 22*. 2001. p. 221–8.
25. Clougherty EV, Pober RL, Kaufman L. Synthesis of oxidation resistant metal diboride composites. *Transactions of the Metallurgical Society of AIME* 1968;**242**(6):1077–82.

26. Nguyen QN, Opila EJ, Robinson RC. Oxidation of ultrahigh temperature ceramics in water vapor. *Journal of the Electrochemical Society* 2004;**151**(10).
27. Monteverde F. The thermal stability in air of hot-pressed diboride matrix composites for uses at ultra-high temperatures. *Corrosion Science* 2005;**47**(8):2020–33.
28. Monteverde F, Guicciardi S, Bellosi A. Advances in microstructure and mechanical properties of zirconium diboride based ceramics. *Materials Science and Engineering A* 2003;**346**(1–2):310–9.
29. Zhang GJ, Deng ZY, Kondo N, Yang JF, Ohji T. Reactive hot pressing of ZrB_2–SiC composites. *Journal of the American Ceramic Society* 2000;**83**(9):2330–2.
30. Fahrenholtz WG. Thermodynamic analysis of ZrB_2–SiC oxidation: formation of a SiC-depleted region. *Journal of the American Ceramic Society* 2007;**90**(1):143–8.
31. Rezaie A, Fahrenholtz WG, Hilmas GE. Evolution of structure during the oxidation of zirconium diboride–silicon carbide in air up to 1500 °C. *Journal of the European Ceramic Society* 2007;**27**(6):2495–501.
32. Sarin P, Yoon W, Haggerty RP, Chiritescu C, Bhorkar NC, Kriven WM. Effect of transition-metal-ion doping on high temperature thermal expansion of 3:2 mullite—an in situ, high temperature, synchrotron diffraction study. *Journal of the European Ceramic Society* 2008;**28**(2):353–65.
33. Yoon W, Sarin P, Kriven WM. Growth of textured mullite fibers using a quadrupole lamp furnace. *Journal of the European Ceramic Society* 2008;**28**(2):455–63.
34. Brennecka GL, Payne DA, Sarin P, Zuo JM, Kriven WM, Hellwig H. Phase transformations in the high-temperature form of pure and TiO_2-stabilized Ta_2O_5. *Journal of the American Ceramic Society* 2007;**90**(9):2947–53.
35. Sarin P, Yoon W, Jurkschat K, Zschack P, Kriven WM. Quadrupole lamp furnace for high temperature (up to 2050 K) synchrotron powder X-ray diffraction studies in air in reflection geometry. *Review of Scientific Instruments* 2006;**77**(9), 093906 1-9.
36. Sarin P, Haggerty RP, Yoon W, Knapp M, Berghaeuser A, Zschack P, Karapetrova E, Yang N, Kriven WM. A curved image-plate detector system for high-resolution synchrotron X-ray diffraction. *Journal of Synchrotron Radiation* 2009;**16**(2):273–82.
37. Sarin P, Haggerty RP, Yoon W, Kriven WM, Knap M, Zschack P. Rapid, in-situ, ultra-high temperature investigations of ceramics using synchrotron X-ray diffraction. In: Rajan Tandon AWEL-C, editor. *Mechanical properties and performance of engineering ceramics. II. Ceramic Engineering and Science Proceedings, vol. 27 (2)*. 2008.
38. ASTM C20-00(2005). *Standard test methods for apparent porosity, water absorption, apparent specific gravity, and bulk density of burned refractory brick and shapes by boiling water*. West Conshohocken, PA: ASTM International; 2005, doi:10.1520/C0020-00R05. www.astm.org.
39. Rietveld HM. A profile refinement method for nuclear and magnetic structures. *Journal of Applied Crystallography* 1969;**2**:65–71.
40. Kriven WM. Possible alternative transformation toughened to zirconia: crystallographic aspects. *Journal of the American Ceramic Society* 1988;**71**(12):1021–30.
41. Heuer AH, Claussen N, Kriven WM, Rűhle M. Stability of tetragonal ZrO_2 particles in ceramic matrices. *Journal of the American Ceramic Society* 1982;**65**(12):642–50.
42. Klug HP, Alexander LE. *X-ray diffraction procedures for polycrystalline and amorphous materials*. 2nd ed. New York, NY: John Wiley & Sons; 1974.